Calibration-Aware Vision-Based Road Friction Estimation with System-Level Braking Analysis

Anonymous Authors

***Abstract*—Accurate road–tire friction estimation is critical for safe motion planning and control in intelligent transportation systems. Vision-based methods typically infer friction by classifying road surface conditions and mapping predicted class probabilities to representative friction levels. While recent approaches report high classification accuracy, they largely neglect probability calibration, despite the well-known overconfidence of modern deep neural networks.**

In this work, we formulate vision-based friction estimation as a conditional expectation over surface classes and analytically show how miscalibrated probabilities propagate into biased friction estimates and amplified uncertainty in braking distance. We quantify this effect through uncertainty decomposition and first-order sensitivity analysis, linking calibration quality to downstream physical risk.

Experiments on a six-class road surface dataset demonstrate that models with comparable classification accuracy can exhibit substantially different calibration behavior, resulting in significant differences in predictive friction variance and stopping distance error. These results highlight that accuracy alone is insufficient for safety-critical ITS applications and that probability calibration must be explicitly considered in vision-based friction estimation pipelines.

I. Introduction

While vision-based friction estimation and deep neural network calibration have both been studied independently in the literature, their joint impact on downstream, physically meaningful quantities such as braking distance remains largely unexplored in the intelligent transportation systems (ITS) context.

The road surface is the only component of the physical environment that interacts directly with the vehicle via the tire–road contact interface. The interaction between tires and pavement determines critical vehicle characteristics, including ride comfort, noise, handling stability, and, most importantly, safety [5, 13]. Accurate and timely knowledge of road condition information is therefore essential for both human drivers and advanced vehicle control systems.

Among various road-related parameters, the peak tire–road friction coefficient plays a particularly crucial role. It defines the maximum longitudinal and lateral forces that can be generated at the tire–road interface and bounds the vehicle's dynamic stability region [18]. Reliable friction information enables human drivers to better assess hazardous conditions and allows advanced driver assistance systems (ADAS) to optimize braking, traction control, and stability management [21]. For highly automated and autonomous vehicles, the requirement is even more stringent: motion planning modules rely on previewed road friction information to generate safe trajectories, while control systems require accurate real-time friction estimates for precise path tracking [8, 19].

Traditionally, road friction estimation has been addressed using vehicle-dynamics-based approaches. These methods process onboard sensor signals such as wheel speeds, accelerations, and steering angles through observers combined with tire and vehicle dynamic models [22]. Variants of Kalman filtering, nonlinear estimation, and particle filtering techniques have been extensively investigated and have demonstrated promising performance in controlled scenarios [11, 16]. However, such approaches inherently estimate friction based on signals collected after the vehicle has already interacted with the road surface. This estimation delay limits their preview capability and reduces their effectiveness for predictive planning in autonomous driving. Furthermore, the strong coupling between tire behavior, vehicle dynamics, and environmental factors makes the inverse estimation problem highly nonlinear and sensitive to modeling assumptions [7].

With the widespread deployment of cameras in production vehicles, vision-based friction estimation has emerged as an attractive alternative. Front-view cameras provide preview information tens of meters ahead, enabling early assessment of road conditions. Recent works leverage deep neural networks (DNNs) to classify road surface states (e.g., dry, wet, snow, ice) from images and infer corresponding friction levels [10, 20, 3]. Large-scale datasets and convolutional neural networks have demonstrated high classification accuracy under controlled conditions [9]. Multi-modal approaches combining vision with additional sensing modalities have further improved recognition robustness [2].

Despite these advances, most existing studies evaluate performance primarily in terms of classification accuracy. However, for safety-critical ITS applications, accuracy alone is insufficient. In many classification-based friction estimation pipelines, friction is implicitly or explicitly derived from predicted class probabilities by associating each surface class with representative friction values. This process assumes that predicted probabilities faithfully reflect the true likelihood of each surface condition.

Modern deep neural networks are known to produce overconfident and miscalibrated probability outputs[1, 14]. A prediction with 90% confidence does not necessarily correspond to a 90% empirical correctness frequency. When such miscalibrated probabilities are directly used to compute expected friction values or to trigger low-friction warnings, systematic bias and unreliable safety decisions may arise even if the overall classification accuracy remains high.

Surprisingly, the role of probability calibration in vision-based road friction estimation has received limited attention. While prior works have focused on improving feature extraction, dataset diversity, and sensor fusion strategies, the statistical consistency of predicted confidence scores is rarely examined.

In this paper, we investigate the role of probability calibration in vision-based friction estimation. We analyze how miscalibrated class probabilities affect friction inference and propagate to braking distance predictions. Experimental results highlight the importance of well-calibrated models for reliable vehicle-level safety assessment.

The main contributions of this work are summarized as follows:

- We formulate vision-based friction estimation as a conditional expectation over road surface classes and derive a probabilistic model that links classification outputs to both friction estimates and their uncertainty.
- Through experiments on a six-class road surface dataset, we show that models with comparable classification accuracy can exhibit substantially different calibration, which translates into significantly different levels of predictive friction variance.
- We demonstrate that better-calibrated models yield more consistent and reliable friction and braking distance estimates, highlighting that probability calibration is a key component of friction estimation pipelines for safety-critical ITS applications.

II. Experimental Protocol

A. Road Surface Dataset

We employ the publicly available RSCD dataset [4], which contains large-scale road surface images acquired under diverse weather and illumination conditions. The dataset provides annotated road surface states, material properties, and road unevenness levels.

For the present study, we reorganize the dataset into a six-class road surface classification problem consisting of: *dry*, *wet*, *water*, *fresh snow*, *melted snow*, and *ice*.

The *dry*, *wet*, and *water* classes include road images with diverse material types such as asphalt, concrete, dirt/mud, and gravel. The distinction between *wet* and *water* corresponds to the presence of a visible water film: the *water* class indicates substantial surface water accumulation potentially leading to hydroplaning, whereas *wet* refers to rainy surfaces without evident water pooling.

The *fresh_snow* class contains newly fallen snow-covered roads, while *melted_snow* represents partially melted snow with mixed surface appearance. The *ice* class includes compacted snow or frozen surfaces associated with extremely low friction levels.

To ensure controlled comparison across models and calibration strategies, we construct balanced splits with:

- 50,000 training images per class,
- approximately 1,750 validation images per class,



Fig. 1: Example images for each road surface class

- 7,000 test images per class.

This balanced configuration prevents class imbalance from influencing friction expectation estimates and enables fair evaluation of probabilistic calibration.

B. Surface Classification Framework

Road surface recognition is formulated as a six-class image classification task. Given an input image x, the objective is to estimate the posterior probability distribution $p(c \mid x)$ over the predefined surface classes.

We employ EfficientNet-B0 as the network architecture due to its lightweight design, and prior work [3] has demonstrated its strong performance for road surface classification tasks. The final fully connected layer outputs six logits z_c, which are transformed into posterior class probabilities using the softmax function:

$$p(c \mid x) = \frac{\exp(z_c)}{\sum_{k=1}^{C} \exp(z_k)}, \tag{1}$$

where $C = 6$.

Training losses. Two training objectives are considered:

- Standard Cross-Entropy (CE) loss,
- Margin-Based Label Smoothing (MbLS) [12], a calibration-aware loss that uses margin-based regularization to improve probability reliability without sacrificing discrimination.

Post-hoc calibration. Independently of the training loss, temperature scaling is optionally applied as a post-processing step [1]. A scalar temperature parameter $T > 0$ is optimized on the validation set, and calibrated probabilities are computed as:

$$p_T(c \mid x) = \frac{\exp(z_c/T)}{\sum_{k=1}^{C} \exp(z_k/T)}. \tag{2}$$

The resulting posterior probabilities are used as inputs to the friction estimation framework described in Section C.

C. Probabilistic Friction Modeling and System-Level Implications

Let x denote an input image and let $p(c \mid x)$ be the predicted posterior probability over surface classes $c \in \mathcal{C}$. Each class c is associated with a physically motivated friction interval $[\mu_c^{\min}, \mu_c^{\max}]$, reflecting the variability of the tire–road friction coefficient observed under that surface condition. Typical friction ranges reported in vehicle dynamics and transportation engineering literature span approximately 0.8–0.9 for dry

asphalt, 0.5–0.7 for wet pavement, and below 0.2 for snow or ice-covered roads [17, 6]. The intervals used in this work are summarized in Table I and lie within these commonly reported ranges.

TABLE I: Friction coefficient intervals for each surface class.

Class	Dry	Wet	Water	Melted_snow	Fresh_snow	Ice
$\mu_c^{\min}$	0.65	0.45	0.30	0.20	0.15	0.10
$\mu_c^{\max}$	0.80	0.70	0.45	0.35	0.25	0.25

a) Probabilistic Friction Model: We model the friction coefficient μ as a conditional random variable defined as a mixture of uniform distributions weighted by the predicted class probabilities:

$$\mu \mid x \sim \sum_{c \in \mathcal{C}} p(c \mid x)\, \mathcal{U}(\mu_c^{\min}, \mu_c^{\max}). \tag{3}$$

The optimal point estimate is chosen as the Bayesian posterior mean:

$$\hat{\mu}(x) = \mathbb{E}[\mu \mid x] = \sum_{c \in \mathcal{C}} p(c \mid x)\, \bar{\mu}_c, \tag{4}$$

where $\bar{\mu}_c = \frac{\mu_c^{\min} + \mu_c^{\max}}{2}$.

Beyond the point estimate, uncertainty quantification is critical in safety-related applications. The posterior variance follows directly from the law of total variance:

$$\mathrm{Var}(\mu \mid x) = \mathbb{E}_c[\mathrm{Var}(\mu \mid c)] + \mathrm{Var}_c(\mathbb{E}[\mu \mid c]). \tag{5}$$

where $\mathbb{E}_c$ and Var_c denote the expectation and variance, respectively, taken with respect to the distribution $p(c \mid x)$.

For the uniform distribution,

$$\mathrm{Var}(\mu \mid c) = \frac{(\mu_c^{\max} - \mu_c^{\min})^2}{12}, \tag{6}$$

while the classification-induced uncertainty is

$$\mathrm{Var}_c(\mathbb{E}[\mu \mid c]) = \sum_{c \in \mathcal{C}} p(c \mid x)\, (\bar{\mu}_c - \hat{\mu}(x))^2\,. \tag{7}$$

For the Bayesian estimator $\hat{\mu}(x)$, the posterior variance equals the minimum achievable mean squared error:

$$\mathbb{E}\left[(\mu - \hat{\mu}(x))^2 \mid x\right] = \mathrm{Var}(\mu \mid x), \tag{8}$$

which provides a theoretically grounded and physically interpretable uncertainty metric.

b) System-Level Illustration: Braking Distance Sensitivity: To illustrate the physical implications of friction estimation errors, we consider a simplified longitudinal braking model. Under standard vehicle dynamics assumptions (flat road, no aerodynamic drag, tire-force saturation), the maximum achievable deceleration is limited by tire–road friction $a_{\max} = \mu g$ [17]. Combining Newton's second law with constant-acceleration kinematics yields the stopping distance

$$d(\mu) = \frac{v^2}{2\mu g}, \tag{9}$$

where v is the initial speed and g the gravitational acceleration.

Since measured friction values are not available in the dataset, the reference friction μ_{ref} is approximated as the mean friction of the ground-truth class, consistent with the probabilistic model definition. The braking distance deviation induced by estimation error is defined as

$$\Delta d = d(\hat{\mu}) - d(\mu_{\mathrm{ref}}). \tag{10}$$

From first-order sensitivity analysis,

$$\frac{\partial d}{\partial \mu} = -\frac{v^2}{2g\mu^2}, \tag{11}$$

showing that braking distance is highly sensitive to friction bias, particularly under low-adhesion conditions. This highlights the safety relevance of accurate and well-calibrated friction estimation. In addition, uncertainty propagation from friction to stopping distance can be approximated through first-order error propagation:

$$\mathrm{Var}(d(\mu)) \approx \left(\frac{\partial d}{\partial \mu}\right)^2 \mathrm{Var}(\mu). \tag{12}$$

Since

$$\frac{\partial d}{\partial \mu} = -\frac{v^2}{2g\mu^2},$$

the variance of stopping distance grows rapidly as friction decreases. Therefore, predictive variance on μ directly translates into amplified uncertainty in braking performance under low-adhesion conditions.

III. Experimental Results

A. Experimental Setup

EfficientNet-B0 is used as backbone with a dropout rate of 0.2. Training is performed for 60 epochs with a batch size of 256 using stochastic gradient descent (momentum 0.9, weight decay 5×10^{-4}).

A One-Cycle learning rate schedule is adopted with a maximum learning rate of 0.1, starting from $0.1/25$ and annealing to $0.1/10000$ following a cosine decay strategy.

B. Calibration Metrics

Model calibration measures the agreement between predicted confidence and empirical correctness. A classifier is well-calibrated if predictions made with confidence p are correct approximately p percent of the time.

Let $\hat{y}_i$ denote the predicted class for sample i, and let $\hat{p}_i = \max_c p_{i,c}$ be the associated confidence, where $p_{i,c}$ is the predicted probability for class c. Given a dataset of N samples, calibration is estimated by partitioning the predictions into M disjoint confidence bins $\{B_m\}_{m=1}^{M}$.In our implementation, the number of bins is set to $M = 15$

For each bin B_m, the empirical accuracy is

$$A_m = \frac{1}{|B_m|} \sum_{i \in B_m} \mathbb{1}(\hat{y}_i = y_i),$$

and the average confidence is

$$C_m = \frac{1}{|B_m|} \sum_{i \in B_m} \hat{p}_i,$$

where $1(\cdot)$ is the indicator function.

The Expected Calibration Error (ECE) [14] is defined as

$$\mathrm{ECE} = \sum_{m=1}^{M} \frac{|B_m|}{N} |A_m - C_m| . \tag{13}$$

Lower ECE values indicate better calibration. Bins with $C_m > A_m$ correspond to over-confident predictions, while $C_m < A_m$ indicates under-confidence.

In addition to ECE, we report Adaptive ECE (AECE)[15], which follows the same formulation but uses bins constructed to contain approximately equal numbers of samples. This provides a complementary view of calibration behavior, reducing sensitivity to uneven confidence distributions.

C. Classification Performance

We evaluate the classification performance of CE and MbLS models on the test set. Results are reported before and after post-hoc temperature scaling (TS), in order to assess both discrimination and calibration properties.

TABLE II: Classification and calibration results .

Model	Acc. ↑	NLL ↓	ECE ↓	AECE ↓	T^*
CE	93.78	0.163	0.724	0.579	1.00
CE + TS	93.78	0.162	0.344	0.379	0.90
MbLS	93.47	0.199	3.40	3.39	1.00
MbLS + TS	93.47	0.179	1.247	1.453	0.80

Both models achieve high classification accuracy, with CE slightly outperforming MbLS. However, calibration metrics reveal a clear difference: CE exhibits significantly lower ECE values both before and after temperature scaling.

Interestingly, although MbLS is designed as a calibration-aware loss, it does not improve calibration on this dataset. One important factor is the nature of the dataset itself. The images are tightly cropped around the road surface, with minimal contextual information. As a result, the classification task is predominantly texture-driven, reducing spurious correlations and limiting overfitting effects. In this setting, the dataset implicitly constrains model confidence, acting as a natural calibration regularizer.

Under these conditions, standard cross-entropy already captures much of the inherent class ambiguity through softmax probabilities. Introducing an additional margin-based smoothing constraint may over-regularize the predictive distribution, artificially reducing confidence levels and leading to systematic under-confidence rather than improved calibration.

This behavior is clearly illustrated in Fig. 2, where the reliability diagram of MbLS shows consistent deviation below the diagonal, indicating under-confident predictions. In contrast, CE remains closely aligned with the diagonal, reflecting better probability calibration.

The optimal temperature values further support this interpretation. For CE, the learned temperature is close to 1 ($T^* = 0.90$), indicating limited miscalibration and only mild overconfidence. For MbLS, a lower temperature is required ($T^* = 0.80$), which sharpens the softmax outputs to compensate for systematic under-confidence introduced during training. This correction is consistent with the reliability diagrams in Fig. 2, which visually confirm that MbLS produces probability estimates that are too conservative before temperature scaling.

Figure 3 shows the confusion matrices for CE. The classes *fresh snow*, *melted snow*, and *ice* are well separated, indicating distinctive visual patterns. In contrast, higher ambiguity is observed between *wet*, *dry*, and *water* surfaces, which share similar appearance and texture characteristics. The same trend is observed with MBLS.This confirms that most classification uncertainty arises from intrinsic visual overlap between specific surface conditions rather than from model overfitting.

D. Friction Uncertainty Analysis

Although the friction point estimate $\hat{\mu}$ remains nearly identical across training objectives and calibration settings, the associated predictive variance exhibits notable differences, highlighting the critical role of calibration in uncertainty propagation.

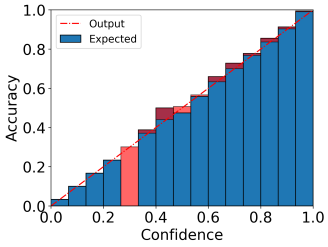
Table III reports the mean friction estimate $\hat{\mu}$, total predictive variance, and Expected Calibration Error (ECE) for CE and MbLS models, before and after post-hoc temperature scaling (TS).

TABLE III: Friction estimation: mean $\hat{\mu}$ and total variance before and after temperature scaling.

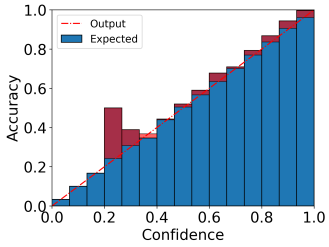
Model	Mean $\hat{\mu}$	Variance	ECE (%)
CE (before TS)	0.4205	0.0050	0.724
CE (after TS)	0.4204	0.0047	0.344
MbLS (before TS)	0.4209	0.0082	3.39
MbLS (after TS)	0.4206	0.0056	1.247

A detailed examination of the results shows that for the CE model, which is intrinsically well-calibrated, the predictive variance is already low before temperature scaling (0.0050) and the ECE is modest (0.724%). After TS, both metrics improve only slightly (variance 0.0047, ECE 0.344%), indicating that the model's probabilities are naturally aligned with observed outcomes. This concentration of predictive friction variance ensures stable and reliable estimates, which is particularly important for downstream vehicle control applications.

In contrast, the MbLS model exhibits higher variance (0.0082) and larger ECE (3.39%) before TS, reflecting under-confidence and diffuse probability distributions across classes. Applying post-hoc temperature scaling substantially reduces both the variance (0.0056) and ECE (1.247%), demonstrating that TS effectively corrects the systematic miscalibration in this model. These results highlight that when a model is poorly calibrated, temperature scaling can significantly improve the reliability and physical coherence of friction estimates.



(a) CE (before TS)



(b) MbLS (before TS)

Fig. 2: Reliability diagrams on the test set before temperature scaling. The blue bars represent the empirical accuracy A_m, while the red segments denote the predicted confidence C_m. Perfect calibration corresponds to alignment with the diagonal ($A_m = C_m$). When the red confidence exceeds the blue accuracy ($C_m > A_m$), the model is over-confident, assigning higher probability than supported by empirical correctness. Conversely, when the blue accuracy exceeds the red confidence ($C_m < A_m$), the model is under-confident.

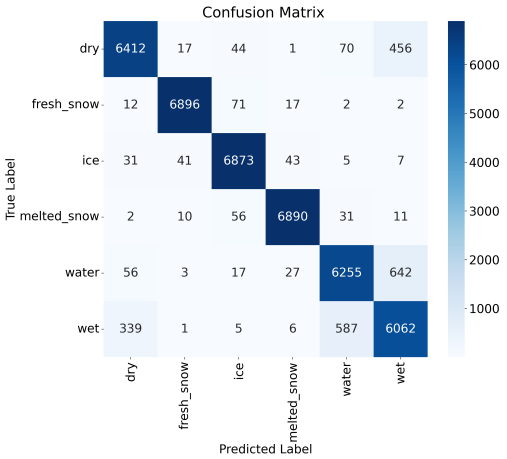


Fig. 3: Confusion matrix of the CE model on the test set

Overall, these observations emphasize that the effect of temperature scaling is strongly dependent on the model's intrinsic calibration. For models that are naturally well-calibrated, such as CE here, TS yields only minor refinements. For models with inherent under-confidence, such as MbLS, TS produces a pronounced reduction in predictive variance, yielding more consistent and physically meaningful friction estimates. This underscores the importance of calibration for generating low-variance, reliable predictions that are suitable for safety-critical intelligent transportation systems.

E. Impact on Braking Distance

We evaluate the effect of model calibration at $v = 25$ m/s (approximately 90 km/h) using the mean absolute and relative stopping distance errors:

$$\text{MABE} = \frac{1}{N}\sum_{i=1}^{N}|\Delta d_i|, \qquad \text{RBE} = \frac{1}{N}\sum_{i=1}^{N}\frac{|\Delta d_i|}{d(\mu_{\text{ref},i})}\times 100\%.$$

Table IV reports these metrics for different models before and after TS.

TABLE IV: Braking distance error at 90 km/h.

Model	MABE (m)↓	RBE (%)↓
CE	2.326	2.57
CE + TS	2.079	2.38
MbLS	5.081	4.61
MbLS + TS	2.815	2.94

Although the average friction estimate $\hat{\mu}$ remains almost unchanged, braking errors vary considerably. MbLS before temperature scaling produces nearly twice the stopping distance error of CE.

This behavior is consistent with the nonlinear relationship $d(\mu) = \frac{v^2}{2\mu g}$. As shown in the sensitivity analysis, stopping distance is inversely proportional to μ and exhibits amplified sensitivity under low-friction conditions. Consequently, increased friction uncertainty leads to larger braking distance deviations.

Temperature scaling substantially reduces MbLS braking error, confirming that probability calibration has direct system-level implications. Even when classification accuracy remains similar, miscalibrated probability distributions increase uncertainty in friction estimation, which in turn amplifies safety-relevant braking errors.

These results demonstrate that calibration quality is not merely a statistical property, but a critical factor influencing downstream physical risk.

IV. Conclusion

This paper examined the impact of probability calibration on vision-based road surface classification for friction estimation in intelligent transportation systems. While classification accuracy is often used as the primary evaluation criterion, we showed that it does not guarantee reliable downstream physical inference.

By modeling friction as a conditional expectation over surface classes, we demonstrated that miscalibrated probabilities directly affect uncertainty propagation in the estimated friction coefficient. Experiments revealed that models with comparable accuracy can exhibit significantly different calibration behavior, leading to noticeable differences in predictive friction

variance, which is critical for downstream planning and control modules that rely on stable friction estimates.

Well-calibrated models, whether obtained intrinsically or through post-hoc temperature scaling, improve probability reliability without altering classification performance and reduce classification-induced friction uncertainty. These results highlight that calibration is a necessary component of classification-based friction estimation pipelines for safety-critical ITS applications.

Although friction ground-truth measurements are unavailable in the dataset, the proposed analytical framework isolates and quantifies the sole impact of probability calibration on downstream physical inference, enabling controlled evaluation of uncertainty propagation effects.

In future work, we plan to develop a complete vision-based friction estimation pipeline that incorporates model calibration as a core component, building upon the probabilistic framework validated in this analysis. We will integrate these calibrated friction estimates with vehicle dynamics models and evaluate their performance in real-time motion planning scenarios.

REFERENCES

[1] Guo et al. "On calibration of modern neural networks". In: *International conference on machine learning*. 2017.

[2] Tianet al. "Multi-sensor fusion based estimation of tire-road peak adhesion coefficient considering model uncertainty". In: *Remote Sensing* (2022).

[3] Tong Zhao et al. "Road friction estimation based on vision for safe autonomous driving". In: *Mechanical Systems and Signal Processing* (2024).

[4] Zhao et al. "A Comprehensive Implementation of Road Surface Classification for Vehicle Driving Assistance: Dataset, Models, and Deployment". In: *IEEE Transactions on Intelligent Transportation Systems* (2023).

[5] Deepak Kumar Dewangan and Satya Prakash Sahu. "RCNet: road classification convolutional neural networks for intelligent vehicle system". In: *Intelligent Service Robotics* (2021).

[6] T. D. Gillespie. *Fundamentals of Vehicle Dynamics*. SAE International, 1992.

[7] Hongyan Guo et al. "A review of estimation for vehicle tire-road interactions toward automated driving". In: *IEEE Transactions on Systems, Man, and Cybernetics: Systems* (2018).

[8] Juqi Hu, Youmin Zhang, and Subhash Rakheja. "Adaptive lane change trajectory planning scheme for autonomous vehicles under various road frictions and vehicle speeds". In: *IEEE Transactions on Intelligent Vehicles* (2022).

[9] Xianjian Jin, Guodong Yin, and Nan Chen. "Advanced estimation techniques for vehicle system dynamic state: A survey". In: *Sensors* (2019).

[10] Felix Kortmann et al. "Modeling the quarter-vehicle: Use of passive sensor data for road condition monitoring". In: *IEEE Sensors Journal* (2020).

[11] Liang Li et al. "Comprehensive tire–road friction coefficient estimation based on signal fusion method under complex maneuvering operations". In: *Mechanical Systems and Signal Processing* (2015).

[12] Bingyuan Liu et al. "The devil is in the margin: Margin-based label smoothing for network calibration". In: *Proceedings of the IEEE/CVF CVPR*. 2022.

[13] Yao Ma et al. "Current non-contact road surface condition detection schemes and technical challenges". In: *Sensors* (2022).

[14] Jishnu Mukhoti et al. "Calibrating deep neural networks using focal loss". In: *Advances in neural information processing systems* (2020).

[15] Jeremy Nixon et al. "Measuring Calibration in Deep Learning". In: *Proceedings of the IEEE/CVF CVPR Workshops*. 2019.

[16] Ashish Pandharipande et al. "Sensing and Machine Learning for Automotive Perception: A Review". In: *IEEE Sensors Journal* (2023).

[17] R. Rajamani. *Vehicle Dynamics and Control*. 2nd. Springer, 2012.

[18] Kanwar Bharat Singh, Mustafa Ali Arat, and Saied Taheri. "Literature review and fundamental approaches for vehicle and tire state estimation". In: *Vehicle system dynamics* (2019).

[19] Lars Svensson et al. "Traction adaptive motion planning and control at the limits of handling". In: *IEEE Transactions on Control Systems Technology* (2021).

[20] Feng Xiao et al. "A novel estimation scheme of tyre–road friction characteristics based on parameter constraints on varied-μ roads". In: *Measurement* (2022).

[21] Shichun Yang et al. "A survey of intelligent tires for tire-road interaction recognition toward autonomous vehicles". In: *IEEE Transactions on Intelligent Vehicles* (2022).

[22] Lei Zuo et al. "Platoon tracking control with road-friction based spacing policy for nonlinear vehicles". In: *IEEE Transactions on Intelligent Transportation Systems* (2022).